Originally published as:

A generalized zero-lag cross-correlation approach for Rapid Earthquake Localization (REL): the example of the Istanbul Megacity Rapid Response System

M. Picozzi[1], C. Milkereit[1], K. Fleming[1,3], E. Çakti [2] and J. Zschau[1]

[1] *Helmholtz Centre Potsdam GFZ German Research Centre for Geosciences, Potsdam, Telegrafenberg, 14473 Potsdam, Germany.*
[2] *Earthquake Engineering Department, Kandilli Observatory and Earthquake Research Institute, Bogaziçi University, 81220 Çengelköy/ Istanbul, Turkey.*
[3] *Department of Spatial Sciences, Curtin University, GPO Box U1987, Perth, 6845, Australia.*

SUMMARY

A seismic antenna approach based on the generalized zero-lag cross-correlation method for rapid earthquake localization is proposed. This method is intended to be applied primarily for early warning, whenever the epicentre-to-target distances guarantee enough lead-time, rapid response purposes, and for those circumstances when a seismogenic area is not directly accessible with seismic stations or/and a network of instruments is concentrated within the area to be warned. The procedure we propose aims to provide useful information for magnitude determination and shake-maps generation. Indeed, it relies only on the first P-wave triggered arrivals from seismic stations, and is designed to work in real time for the localization of events occurring outside of the network, that is, under conditions that might be detrimental to standard localization approaches.

The procedure can by summarized by a few preliminary pre-seismic and real-time co-seismic steps. In the pre-seismic time-frame, for the cases where a large and dense network exists, waiting for all stations to trigger could dramatically reduce the available lead-time for the warning. Therefore, in such cases the network could profitably be divided into sub-arrays, while also taking advantage of available earthquake recordings or simulated data-sets.

During the co-seismic time-frame, the main operations are: 1) individual on-site triggering by the P-wave of the seismic stations (e.g. by a STA/LTA algorithm); 2) real-time communication of key parameters (e.g., P-wave arrival time, and signal quality) to a main centre by SMS/WLAN; 3) setup of a pseudo data set, composed by a Gaussian function centred at the P-time, and with a bell width that can be set up proportional to the trigger signal-to-noise ratio (SNR); 4) calculation of a coherency map for the sub-array with triggered stations (preliminary sub-array location); and 5) stacking of coherency maps from the different sub-arrays (final location). By the stack of coherency maps estimated by the different sub-arrays in the last step of the procedure, the epicentral area's location may be better constrained. This innovative approach for rapid localization was applied to both synthetic data, and real observations of two small earthquakes that occurred in the Marmara Sea, Turkey, which were recorded by the Istanbul Earthquake Rapid Response System.

Abbreviated title: Rapid Earthquake Localization

Corresponding author:

Matteo Picozzi, GeoForschungsZentrum, D-14473, Potsdam, Germany

Phone: +49-331-2881285

FAX: +49-331-2881204

e-mail: picoz@gfz-potsdam.de

1 Introduction

Seismic early warning (EW) and rapid response (RR) systems that are being developed or already exist worldwide (e.g., Japan, Taiwan, Mexico, Italy, Turkey, California, etc.; Allen and Kanamori, 2003; Kanamori, 2005) represent a valuable component of seismic risk mitigation strategies, particularly for megacities. In fact, recent technological and communication advances have allowed the development of networks that are able to rapidly perform seismological analysis of ground motion during and after a strong earthquake for the purpose of EW and RR. A fundamental piece of information for the estimation of potentially strong earthquake ground motion severity is a reliable first estimate of the epicentre location.

In contrast to post-event localization procedures that rely on both P-wave and S-wave arrival times, and for which the computation time is not a constraint, a localization procedure for real-time EW and RR systems must be an optimal compromise between the precision of the obtained result and the time, clearly as small as possible, needed for the analysis.
For this reason, EW and RR localization approaches often rely only on the P-wave arrival times, and the design of localization procedures for real-time purposes tries to reduce the computational time, while at the same time obtaining a reasonable level of precision in the results. Furthermore, EW and RR methods also typically take into account the existence of seismological and geometrical constraints (e.g., the existence of a known source area, the distance of the seismogenic area from the site to be warned, technical characteristics and geometry of the network, etc.).

Recently, successful efforts in the development of real time localization procedures have been obtained for 'regional early warning systems', that is to say networks of seismic stations located around well-known seismogenic areas that are located at a distance from the site to be warned that allow a useful lead time (e.g., Satriano *et al.*, 2008; Allen, 2007). These authors showed that in such cases, a reliable event localization is also successfully achieved with only a few seismic stations, which are opportunely located in the immediate vicinity of the seismogenic area. Hence, in these cases the warning procedures take advantage of the distance between the seismogenic area and the site to be protected, and of the different seismic phases velocity (i.e. P-waves about 6-7 km/s, S- and surface waves about 3.5 km/s).

On the other hand, when different situations must be faced, such as the presence of a seismogenic area not directly accessible with seismic stations (e.g., faults placed offshore) or/and the existence of a network of instruments concentrated within the urban area to be warned, which is a quite common condition for 'on-site early warning systems', methods based on the analysis of P-wave arrival times might suffer from resolution problems due to the source-array geometry. In such situations there is, in fact, an irresolvable trade-off between the unknowns (e.g., origin time, hypocentre depth, and spatial coordinates) of the localization inverse problem.

A very interesting case of the latter is represented by the Marmara Sea Region, Turkey, where a network of accelerometric stations (i.e., the Istanbul Earthquake Rapid Response System, IERRS) is located within Istanbul, while potential seismogenic faults are located at a close distance under the Marmara Sea (e.g., Erdik *et al.*, 2003a). With this regard, Figure 1 illustrates what happens when a standard localization procedure such as Hypoellipse (Lahr, 1999), a well-established location algorithm, is used with the IERRS arrival-time data-set in order to locate the epicentre of an earthquake occurring outside of the network. Considering an event that occurred in the Marmara Sea on September 29th, 2004 (see section 4 for further details about this event) and using the 1D velocity model proposed by Karabulut *et al.* (2002) (Table 1), Figure 1a presents the inversion results provided by Hypoellipse for the cases when only the P-wave arrival times are used and when both the P and S wave times are considered. Usually, in order to provide information about the error associated with the localization estimate, the standard error ellipse produced by Hypoellipse is shown. The confidence region computed by Hypoellipse is normally associated with a 68% level of confidence, and is evaluated by combining the partial derivatives of the spatial location at the final hypocenter, and the standard error estimates for the arrival times (Klein, 2002). For the analyzed data-set shown in Figure 1, we have adjusted the size of confidence regions to correspond to a 95% level of confidence, where the ellipsoid errors' semi-major and -minor axes lengths associated with the inversion solutions are still relatively small (i.e., 1.1 km and 0.84 km when inverting using only P-wave arrival times, respectively, and 0.2 km and 0.16 km, respectively, when both P- and S-wave arrival times are considered). Despite the Hypoellipse estimates being associated with relatively small error ellipses, which in the case of the P and S times inversion cannot be properly visualized at the scale of Figure 1a, for both cases (i.e., P-wave and P- and S-wave inversions) the solutions are several tens of kilometres from the reference solution obtained by Atakan and Sorensen (2006) and Birgören and Özel (2006). Hence, it is likely that Hypoellipse remained trapped in some local minimum of the inverse problem. An in-depth discussion on the reasons for the unsatisfactory Hypoellipse performance is beyond the scope of this paper. From our point of view, this example clearly outlines that the particular geometry of the IERRS network limits the ability to correctly locate an earthquake's epicentre using methods based on the inversion of P-wave arrival times. Indeed, we find that under more favourable 'geometrical' conditions, that is when both P and S-wave arrival times recorded by the IERRS stations and, in particular, an additional 7 seismological stations distributed around the Marmara Sea (obtained from the International Seismological Centre database) are considered (Figure 1), the Hypoellipse location is almost coincident with the reference one. However, the use of stations located far from the seismic sources, while allowing an improvement in the location precision, is incompatible with the short lead time requirements of EW and RR systems.

An effective approach that allows a reduction in the trade-off between the inversion problem unknowns (origin time, hypocentre depth, and spatial coordinates) is to work on the experimental arrival time differences at the network stations, and their comparison with theoretical time differences computed for different hypothetical sources. A similar approach was proposed by Krueger and Ohrnberger (2005), and consists of discretizing the source region of interest into a grid of possible epicentres. Then, for each hypothetical source, the P-

wave travel times at each station are computed taking into consideration a homogeneous velocity crustal model considered representative of the area, and stored as time-differences in a lookup table. Hence, during an event, once a data set of the experimental P-wave arrival times is available, the root mean square between the vectors of experimental and theoretical time-differences is used to locate the epicentral area. A further advantage of such an approach is that the computational time is very limited. On the other hand, possible drawbacks of the method include heterogeneities in the crustal structure, and the presence of noise corrupting the arrival time estimates.

A possible alternative strategy for rapid earthquake localization in situations like that of Istanbul and its IERRS network involves adopting a seismic antenna approach. In the post-event time frame, seismic antenna approaches based on waveform correlation analysis have been successfully used for several decades for earthquake localization and identifying earthquakes' rupture propagation evolution (e.g., Ringdal and Kvaerna, 1989; Goldstein and Archuleta, 1991; Fletcher *et al.* 2006; Krüger and Ohrnberger, 2005; Gibbons and Ringdal, 2006). In this work, we propose a seismic-array based approach for Rapid Earthquake Localization (REL) adapted to the real time demands of RR systems. REL is based on a combination of standard, robust seismic antenna approaches and relies only on the first P-wave triggered arrivals. In particular, the zero-lag cross-correlation method (Frankel *et al.*, 1991) has been implemented, including improvements introduced by Almendros *et al.* (1999) that allow the wave-front to be circular, making the method also effective for the case of nearby sources. Moreover, to make the procedure appropriate for large, poorly coherent regional arrays (where the waveforms at different sensor sites are not similar, precluding robust parameter estimates from standard waveform correlation methods) an analytical normalized Gaussian function centred on the estimated P-wave phase arrival time for each sensor is adopted. The localization procedure is optimised by adopting a multi-cluster approach, as proposed by Almendros *et al.* (2001a, 2001b), where a large and sufficiently dense seismic network (i.e., some tens of sensors deployed over a range of tens of kilometres) is first divided into different sub-arrays. Then, the estimated parameters obtained by REL for each sub-array are stacked and, similarly to a triangulation procedure, a final real time localization of the source epicentral area is obtained.

The availability of information in real-time is the fundamental requirement of any EW or RR system. Hence, the REL method also relies on the capability of acquiring in real time P-wave trigger times from the network's stations at some main centre where the REL analysis can be performed. Furthermore, thanks to recent advances in communications technology, analysis strategies such as REL are nowadays possible. For example, the *Helmholtz Centre Potsdam GFZ German Research Centre for Geosciences* (GFZ Potsdam) and the *Humboldt University of Berlin* (HUB) have recently developed for seismic early warning purposes a self-organizing wireless mesh information network made up of low cost sensors. A test version of this system, referred to as the Self-Organizing Seismic Early Warning Information Network (SOSEWIN), consisting of 20 sensors, has been deployed since July, 2008, in Istanbul, Turkey, with the aim of setting up a new earthquake early warning system for the mega city (Fleming et al., 2009). Preliminary tests of the SOSEWIN's communications performance

have shown that real-time transmission of estimated ground motion parameters is possible (Fleming et al., 2009). Therefore, the REL method has been developed with the aim of being integrated as one of the localization strategies used in systems such as SOSEWIN.

As stated above, Istanbul already hosts the IERRS system, a dense strong motion recording network consisting of 100 stations for rapid response and early warning purposes (Erdik *et al.* 2003b). The system has been developed by the *Kandilli Observatory and Earthquake Research Institute* (KOERI) of *Bogazici University*, in collaboration with the Governorate of Istanbul, the First Army Headquarters and the Istanbul Metropolitan Municipality. The strong motion stations are located in densely populated settlements within the metropolitan area of Istanbul, and operate in dial-up mode for rapid response information generation. The relative instrument spacing between the stations is about 2-3 km, and the stations are located at ground level in small and medium-sized buildings. When triggered by an earthquake, the IERRS stations process the streaming three-channel strong motion data to yield information about P-wave arrival times, spectral acceleration at specific periods, and 12 Hz filtered PGA and PGV values, and forwards these parameters in the form of SMS messages directly to the main data centre through the GSM communication system (see Sesetyan *et al.,* 2010, for further information about the IERRS network methods and practices).

In this study, the REL procedure performances have been evaluated using the IERRS system as a reference. In particular, the method is tested using synthetic data, and then by real strong-motion data recorded by the IERRS from two moderate events that occurred in the Marmara Sea region during 2004. Furthermore, the results of the REL method have been compared with those obtained by Hypoellipse and by the use of a LookUp Table procedure (hereafter LUT) similar to the one proposed by Krueger and Ohrnberger (2005).

2 Methodology

The core of the REL procedure is based on the zero-lag cross-correlation (ZLC) method proposed by Frankel *et al.* (1991), which was found to be effective within several different contexts for the analysis of various types of seismic signals (see, e.g.,, Mori *et al.*, 1994; Del Pezzo *et al.*, 1997; Almendros *et al.*, 1999). One advantage of the method is that, differently from methods based on Fast Fourier Transforms (FFT), ZLC is independent of the time window length, and hence can be applied to very short duration signals, such as an earthquake's first arrival.

The method consists of measuring the cross-correlation in the time domain between signal pairs, which is defined as.

$$R_{jk}(\tau) = \left\langle W_j(t) \circ W_k(t + \tau) \right\rangle, \qquad (1)$$

where j and k represent a station pair, $W_j(t)$ is the seismic trace at station j, the symbol $\langle ° \rangle$ indicates the time average, and τ is the time delay between the stations j and k. Usually the average cross-correlation coefficients R_{jk} are normalized over all sensor pairs

$$R = \frac{1}{N^2} \sum_{j,k=1}^{N} \frac{R_{jk}(\tau_{jk})}{\sqrt{R_{jj}(0)R_{kk}(0)}} . \qquad (2)$$

Practically, the aim of the ZLC method is to find the shift τ_{jk} among the pairs of traces for which the function R is the maximum. The shift τ_{jk} is itself a function of parameters characterizing the epicentre location (i.e., the apparent slowness vector $\mathbf{S} \equiv (S_x, S_y)$ which depends on the velocity structure in the area between the epicentre and the network, and in polar coordinate, the backazimuth A between the sensor network's barycentre and the epicentre). Therefore, to find the value of τ_{jk} that maximizes the function R, we must find the parameters A and $\mathbf{S}$ that constrain the earthquake's epicentre location (Del Pezzo *et al.*, 1997).

In particular, following Almendros *et al.* (1999), τ_{jk} as a function of A and $\mathbf{S}$ is given by:

$$\begin{aligned}
\tau_{jk} = t_k - t_j &= (x_k - x_j)S_x + (y_k - y_j)S_y \\
&= \mathbf{S} \, [(x_j - x_k)\sin A + (y_j - y_k)\cos A]
\end{aligned} , \qquad (3)$$

where $\mathbf{S}$ is equal to $\sqrt{S_x^2 + S_y^2}$, and A is equal to $\tan^{-1}(S_x / S_y)$.

The ZLC method, as proposed by Frankel *et al.* (1991), operates under the strong assumptions that (1) a plane wave front is propagating across the array, and (2) there are no site effects affecting the signal at any station. Clearly, both assumptions limit the applicability of the procedure to only a restricted number of cases.

In particular, the assumption of a plane wave-front is not reliable if the distance of the source is not large enough compared to the array size. Hence, in order to make the method more flexible, Almendros *et al.* (1999) generalized the computation of the time delay between stations to take into account the case of a circular-wave-front, which can be expressed as a function of $\mathbf{S}$, A and the distance D between the epicentre and the sensor network's barycentre. Thus, following Almendros *et al.* (1999), τ_{jk} is given by:

$$\begin{aligned}
\tau_{jk} = \mathbf{S} \, (&\sqrt{(x_k - D\sin A)^2 + (y_k - D\cos A)^2} \\
&- \sqrt{(x_j - D\sin A)^2 + (y_j - D\cos A)^2})
\end{aligned} \qquad (4)$$

Equation (4) remains valid for the case of a source at depth and for vertically inhomogeneous medium, since under such conditions the intersection of the wave front with the surface is still

circular. The effectiveness of this 'generalized ZLC' was demonstrated by Almendros *et al.* (1999) by the estimating the epicentre locations of seismo-volcanic sources at Deception Island, Antarctica, relative to a nearby seismic array. Similarly, working on tele-seismic signals and large aperture arrays, Kruger and Ohrnberger (2005) observed and discussed the presence of artifacts affecting location estimates when working with plane wave front approaches and large networks. Therefore, these authors adopted a non-plane wave approach that takes into account the curvature of the wavefronts, and observed that with this approach, larger apertures and a broader frequency ranges can be used without distorsion.

The absence of local site effects is the second strong, and limiting, assumption required by the ZLC method. Recently, Gibbons *et al.* (2008) showed that in the case of large inter-station distances associated with significant geological heterogeneity, which is a common feature of large networks, the waveform dissimilarities strongly limit the efficiency of standard seismic array analysis approaches. For this reason, these authors proposed the use of transformed spectrograms in waveform analysis at different frequencies. Of course, these powerful approaches are not suitable for the typical time frames of concern in RR and EW. Although we consider it very important to manage the non-coherent nature of the signals detected by large arrays, it must be remembered that EW and RR systems, when applied to situations where the distance between the seismic source and the site-to-be-protected is very short, cannot "wait for", nor be "based on", the transferring of complete waveform data and their spectral analysis to be efficient. This is the reason why, in order to make our procedure appropriate for large, poorly coherent regional arrays and rapid response activities, we decided to rely only on P-wave arrival times. The best option for EW and RR activities is therefore represented by the local analysis at each station of the data streaming for the event detection. Hence, after the triggering of a station only a few key parameters are transferred towards the main centre where early warning and rapid response activities and decisions are carried out, including of course the P-wave trigger times *tp* (Erdik *et al.,* 2003b; Fleming *et al.,* 2009). Therefore, while classical earthquake localization algorithms operating in the post-event timeframe can take advantage of a precise determination of arrival times for different seismic phases (i.e., P- and S-waves) and also use observations from more distant seismic stations that, owing to their positions, allow the improvement of the precision of the location results (see Figure 1), the REL approach is designed to rely only on the first P-wave arrival times automatically detected from the monitoring of the vertical component of ground motion at each sensor (hereafter *P-time*) of an 'on-site' EW and RR system.

In particular, once the *P-times* are transmitted from the stations that detected the earthquake to the main centre, the generalized ZLC analysis is performed using analytic normalized Gaussian functions substituting the original seismograms. The Gaussian 'bell' shape has been selected as the synthetic signal for the computation of the ZLC because of its simplicity and dependence on only two parameters, which can be easily linked to the signal's characteristics. The first parameter, which regulates where the Gaussian function is centred, is defined as the *P-time*, while the second parameter controlling the bell's width can be defined as being proportional to the signal-to-noise ratio at the moment of the P-wave trigger, which

accommodates the uncertainty in the trigger timing due to the noise conditions at the seismic station. Clearly, since it is based on the *P-time* values, the effectiveness of the REL procedure will also be dependent upon the detection procedure implemented in the network. Thus, as for all EW and RR systems, the selection of a good automatic picker algorithm is an important step. However, the use of a Gaussian window centred on the P-wave trigger time helps to reduce the influence of associated timing errors. In this work, for the analysis of the experimental datasets, we implemented into REL the standard and robust recursive STA/LTA trigger algorithm (Schweitzer *et al.,* 2002). However, any equivalent algorithm could be used.

In order to optimise the localization estimates, we followed a procedure similar to Almendros *et al.* (2001a, 2001b), where different portions of the network are used as sub-arrays (i.e., clusters of sensors). In fact, if the different sub-arrays can detect the event from different azimuths, a procedure equivalent to triangulation can be implemented to spatially constrain the epicentral area. In practice, the epicentral coherency maps obtained by different sub-arrays are stacked step-by-step. In this way, problems due to the presence of local spurious coherency maxima affecting single array analysis or eventual bias effects along particular backazimuths due to the sub-array's geometry are reduced, and the resultant redundancy of information makes the maximum in the final coherency representation a more reliable and robust estimate of the epicentral area. Figure (2) provides a flowchart that represents a schematic overview of REL as designed and implemented in this work for the IERRS strong motion data. First, within a pre-seismic time-frame, the IERRS network is divided into different clusters (i.e., sub-arrays) consisting of about the same number of stations. The division of the network into sub-arrays can be performed following different criteria (e.g., geographical constraints due to the distribution of station with respect to the location of a seismogenic area, or communication constraints). In the case of the IERRS network, the sub-arrays' numbers of stations and shapes were selected in order to reduce as much as possible the horizontal azimuthal gap in the Marmara Sea, which from previous studies (e.g., Armijo *et al.,* 2005) is expected to be a possible epicentral area for a future large-magnitude earthquake of Mw ≈ 7. Of course, the optimal configuration of sub-arrays might be determined also by taking advantage of simulations or data-set from previously recorded events.

In the event of the occurrence of an earthquake in the Marmara Sea, the co-seismic operations will start with the communication of the *P-time* detected at each station by their STA/LTA algorithm towards a main centre, which we hypothesize to be KOERI. Therefore, analytical Gaussian signals centred on the *P-time* and having a width that can be dependent upon the noise affecting the recording are used as input to the ZLC analysis (Figure 3).

Following Almendros *et al.* (1999) for the case of a circular-wave-front geometry, the time delay between stations becomes a function of the parameters' backazimuth, apparent slowness and epicentral distance. Considering that a 3-D grid search to solve the three parameters simultaneously would be computationally demanding, Almendros *et al.* (1999) suggested doing so step-by-step. Following their scheme, a grid search using the plane wave approximation is first performed to constrain the apparent slowness. Then, keeping fixed the apparent slowness, a 2-D grid search for the selected azimuths and epicentral distances is

carried out using the circular wave-front geometry. By means of these operations, a map of coherency estimates for a variety of possible source azimuths and distances along a pre-defined grid centred to the geographical IERRS barycentre is obtained for each cluster (Figure 2). Finally, the azimuth-distance coherency maps of different clusters are stacked, simulating a triangulation scheme, and hence allowing the epicentral area corresponding to the location with the highest coherency value to be identified (Figure 2). It is worth noting that the grid search dealing with the optimal azimuth and epicentral distance is flexible and can be adjusted for different situations. For example, implementing REL for the IERRS system, we decided to limit the search area to the Marmara Sea (Figure 2). In fact, the whole area south of Istanbul is considered a region where the probability of a major earthquake occurring over the next few decades is high, especially with respect to the low seismicity area of the Black Sea located north of the mega city. Furthermore, concerning the optimization of REL for the Marmara region's seismic threats, we undertook an addition step by focusing the coherency search only on those points located along schematic representations of the seismogenic faults (e.g., Armijo *et al.,* 2005) in the Marmara Sea. This latter approach allows a considerable reduction in the computation time required for the coherency estimation, and thus permits REL to be useful, with respect to most of the considered faults, for EW purposes.

Differently from the classical seismological approach used to locate seismic events, which require for the inversion of the arrival times an average velocity model representative of the whole area between the source and the stations, an advantage of REL is that it does not involve an inversion stage that is dependent upon a particular velocity structure. In fact, in the first stage of the procedure, an average slowness value representative of the area is automatically obtained from the *P-time* data set. On the other hand, as with all early warning methods, REL also possesses certain drawbacks. For example, as with other seismic antenna approaches, strong lateral velocity variations below the sub-arrays could lead to anomalous delays of *P-times* between stations. In these cases, it would be impossible to obtain high-quality epicentre location estimates. However, the presence of lateral velocity variations under a sub-array causes negative effects independent of the importance of the event being analyzed. Thus, such more complex cases could be identified *a priori* by a training period of the REL method using lower magnitude events, allowing the REL's efficiency during stronger events to be assured.

3 Application to synthetic data

In order to verify the effectiveness of the REL procedure, tests employing synthetic data were performed using the IERRS network and the Marmara Sea region as a reference. First, different possible epicentres along schematic seismogenic faults located within the region of concern were hypothesized (Figure 4). Some of these modelled scenarios correspond to epicentres of events that had struck Istanbul in the past (e.g., event 1 mimics the 1999 M 7.4 Izmit Earthquake, and event 7 simulates the 1912 M 7.4 Earthquake in Ganos). Next, assuming a common depth of 10 km for all the scenarios and using the P- and S-wave

velocity model proposed by Karabulut *et al.* (2002) (Table 1), theoretical P-wave arrival times were computed for the IERRS stations by the program TauP (Crotwell *et al.,* 1999). Finally, these *P-times* data sets are used as input for the REL strategy.

During these tests, the STA/LTA trigger operation was skipped, since for synthetic data this step was considered unnecessary as our main interest here was to test the capability of the proposed ZLC analysis when applied to *P-time* data for rapid event localization. Figure (4) shows the results from the first series of scenarios performed using a grid search that spans the whole area south of Istanbul and which aims, under the requirements of a RR system, to be a good balance between computational time and an acceptable accuracy in the localization. This involved using steps of 5° degrees for the azimuth, and steps of 5 km up to 150 km in distance from the IERRS barycentre.

The epicentres of the selected scenarios were found to be very well retrieved by REL. That is, with the exception of scenarios 1 and 7, which are located east of the network (Figure 4), the areas with the higher coherency values (i.e., scenarios 2, 3, 4, 5, and 6) are grouped around the modelled epicentres. These results suggest that REL provides reliable event locations that could represent an important piece of information for RR systems. However, at the same time, the results from the synthetic tests indicate that along particular azimuths, the IERRS network's geometry could affect the REL's resolution in estimating the epicentres' true distance. Therefore, in order to evaluate the general performance of the IERRS network when it is used as a 'seismic antenna' in the REL procedure, we followed the approach of Almendros *et al.* (1999), and simulated different datasets of *P-times* for isotropic sources (≈ 2300) distributed over a range of azimuths and distances on a regular grid in polar coordinates (i.e., the individual dots shown in Figure 5). This test was carried out considering steps of 5° degrees for the azimuth, and steps of 2 km for distances less than 10 km from the IERRS barycentre, and of 5 km for distances up to 150 km.

Figure (5) shows the percentage error in both the inferred distance and azimuth when locating the source (i.e., *100 ×·(real value-estimated value)/real value*). Our results indicate that the errors for the azimuth values (Figure 5a) are generally less than 10%, with a few exceptions in the case of sources located practically inside the network, for which, in any case, effective EW activities would not be able to be carried out. Similarly, the epicentral distances are in general well estimated and characterized by errors less that 20%. However, along particular azimuths, the estimated epicentral distances may be affected by significant errors, such as for far-field sources located along narrow azimuthal ranges, where, due to the geometrical characteristics of the IERRS, the three different sub-arrays share nearly the same back-azimuth with respect to the source position, making the triangulation results unstable (Figure 5b). However, for such cases, the error associated with the azimuth is nonetheless still fairly small (i.e., less than 10%). This tells us that when REL is applied to the IERRS network, due to the network's geometry, for sources located in these two sectors, we must be aware that although the inferred distances could be severely over- or under-estimated, the azimuths will still be well constrained. Finally, for grid points corresponding to possible source locations

along the North Anatolian Fault Zone in the Marmara Sea (i.e., located directly south of the IERRS network), REL is able to provide epicentre estimates that are characterized by small uncertainties in both the azimuth and distance estimates.

Taking into account that the distribution of seismogenic faults in the Marmara Sea Region is very well characterized (e.g., Armijo *et al.,* 2005), we also explored the REL's performance when it was focused on monitoring only those faults located south of Istanbul. Figure (6) shows the REL results obtained for some of these scenarios. We note that this application of the REL method provided excellent event location estimates, with the advantage of a smaller computation time (i.e., between 2 and 3 sec., depending upon the given computer's capacity).

Therefore, with the exception of that branch of the North Anatolian Fault located just south of Istanbul (i.e., scenario 1, Figure 6) for which the warning time is very small (i.e., only about 2 seconds), REL was able for all the other faults to provide a first epicentre estimate that, while from a purely seismological view may seem somewhat inaccurate, is nonetheless almost instant and sufficiently precise to be exploitable for a rapid computation of the event's magnitude during EW activities.

Finally, using the same synthetic data set, tests were performed to evaluate the performance of REL when applied to the IERRS network in the event of malfunctioning stations. For this test, we adopted a Jacknife Analysis (Efron and Gong, 1983) which is a modern statistical technique that has been proposed to quantitatively determine the error bound for specific model parameters. In brief, the Jacknife method consists of repeated inversions (50 times in our case) while considering several datasets, termed samples, obtained by randomly deleting a certain amount of information from the original dataset, that is eliminating randomly selected stations from each sub-array. Hence, for each iteration we defined the error in the localization in azimuth and distance, and their sum, between the true and the reconstructed epicentre location. Figure (7) shows the results of the Jacknife Analysis performed using different thresholds for the random elimination of stations (i.e., until the number of stations has been reduced to 50% of the original) in each sub-array. For each Jacknife analysis, we computed the average and the 95% confidence interval of each kind of error. We find that for the IERRS network, the total error in the localization provided by REL is less than 5% when using all available stations, and is also the case when 25% of the stations in each sub-array are eliminated (Figure 7). This demonstrates the considerable robustness of the REL method in providing a reliable epicentre estimate. It is worth mentioning that similar tests of the REL's efficiency could be used as *a priori* assessments of the possible performance of REL for any other arrangement or kind of seismic network.

4. Application to real-data sets

We next apply the REL procedure to the data sets collected by the IERRS network for two events that occurred along the releasing bend of the North Anatolian Fault Zone in the

Marmara Sea. Figure (8a) shows the location of the IERRS stations and the moment tensor solutions of the May 16, 2004 (Mw = 4.1) and September 29, 2004 (Mw = 4.1) events. Figure (8b) shows, as an example, the accelerograms recorded at the IERRS stations during the first earthquake. It is important to note the influence of local site conditions and geological heterogeneity across the network, potentially leading to significant waveform changes between different sites, a point that has been well documented in several studies (see e.g., Tezcan *et al.*, 2002; Ozel *et al.*, 2004; Ansal *et al.*, 2004, Picozzi *et al.* 2009). For example, note the larger amplitude and length of the time of ground shaking in the western part of the city with respect to some stations close to the Bosphorus channel in the eastern part. These observations confirm the incoherence of the IERRS signals, and that robust estimates from classical waveform correlation approaches relying on the original seismic signals might not be possible. On the other hand, problems due to site effects are partially overcome in REL by using the Gaussian functions centred on the *P-time*.

Since these tests involve the analysis of real data from the IERRS, the REL procedure is implemented in a more general algorithm that includes the simulation of the synchronized real-time data flow (based on the sampling rate of 200 Hz used by the IERRS stations) and the real-time event detection of the event by the recursive STA/LTA trigger (Schweitzer et al., 2002). Figure (9) shows some examples of the STA/LTA performance with data from the two events. The automatically determined *P-times* are observed to be generally accurate. Therefore, during these tests we decided to keep the Gaussian window width constant and equal to 0.2 seconds (Figure 3). It is worth noting that, as for any localization method, under real conditions any error in the *P-time* arising from the performance of an automatic picking algorithm will be transferred to the REL results. Moreover, an additional source of uncertainty is due to the availability of a smaller number of stations operating at the time of the earthquakes with respect to the complete IERRS network (70 stations for the first event, and 79 stations for the second).

It can be seen from Figures (10) and (11) that even under these unfavourable, but nonetheless realistic, operational conditions, REL provides epicentral location estimates that agree well with those obtained from the post-event application of classical methods (e.g., Atakan and Sorensen, 2006; Birgören and Özel, 2006) that also make use of seismological stations distributed around the Marmara Sea. In particular, it is interesting to note that while the coherency maps of the single sub-arrays for the September 29, 2004 event (Figure 10a) provide an accurate indication of the event's backazimuth, but fail to estimate the correct epicentral distance, Figure (10b) shows that when the sub-array's coherency maps are combined, the distance to the epicentre is very well constrained. In fact, the differences between the REL and standard localization estimates of epicentral distance and azimuth with respect to the IERRS barycentre location are for this event 8.2 km and 4° degrees, respectively.

Figure (10c,d) presents the results obtained when REL is applied while focusing only on the seismogenic faults in the Marmara Sea area. Here, the results obtained by REL are in

excellent agreement with the reference localization, and the differences in the distance and azimuth for the two estimates are 4.3 km and 1.5°, respectively. These discrepancies between results obtained using the REL and standard localization approach depend on the uncertainty that affects both methods. For instance, the sources of error for REL, which have been discussed in the previous sections using synthetic data (i.e., failing of stations, errors in the P-wave arrival time, and lateral velocity variations below the sub-arrays), have, of course, even greater importance when the method is applied to real data. However, we stress again the point that the aim of REL is to provide a first estimate of the epicentre localization for the case of events occurring around a network of seismic stations. That is, to provide useful information for RR systems, and eventually for EW for the case of large source-to-site distances. In fact, we remind the reader that the quality of the REL results must be evaluated within the context that the procedure does not aim to be a substitute for other classical seismological localization approaches. On the contrary, it is designed to be applied under those critical real-time conditions where the availability of even an approximate epicentre location would allow some form of rapid response analysis (e.g., shake map computation) and, in the event of large source-network distances, possibly allow the implementation of early warning mitigation activities. Interestingly, Figure (11) shows that very similar results are also obtained when the same data-set is analyzed using a LUT approach (i.e., estimates of epicentral distance and azimuth with respect to the IERRS barycentre location are in this case 3 km and 2.5° degrees, respectively). We point out that the theoretical arrival times for the grid of hypothetical epicentre have been computed in this case by the procedure described in the section 3, while the best location is found as the maximum of the RMS^{-1} function. Moreover, although none of the code adopted in this work is optimized and they are running on a standard PC, we observed that both the REL and LUT approaches provide results within a few seconds (i.e., about 5 seconds REL, between 2 and 3 seconds REL with search points along the main faults and LUT).

Clearly, the time lost for computation must be added to the time necessary for the triggering of the stations within a sub-array, and to that necessary for the communication of the *P-times* from the stations towards the main centre. Considering that the sum of these three terms is lost from the available lead-time, it must be recognized that while the latter does not affect the usability of REL and LUT approaches for RR purposes, for certain event locations the loosing of only few seconds might be critical, making it impossible to issue in time EW messages.

Figure (12) shows that for the Map 16, 2004 event, which occurred close to the Yalova peninsula, the REL results are also in agreement with the reference epicentre. In this case, the discrepancies in the estimated distance and azimuthal values from the REL with respect to the reference localization are 9.5 km and 2.4°, respectively (Figure 11b), and when focusing only on the seismogenic zones in the Marmara Sea area are 3.6 km and 0.5° (Figure 11d), respectively.

Finally, we decided to verify the REL performance by carrying out a direct comparison of its results with those obtained using Hypoellipse (Lahr, 1999). For this test, we decided to focus on the September 29, 2004 (Mw = 4.1) event, and used the 1D velocity structure for the area proposed by Karabulut *et al.* (2002). In order to mimic the cluster approach of REL, we

estimated the Hypoellipse epicentre location three times using the P-wave arrival times of the different sub-arrays (i.e., the same sub-arrays used by REL). Figure (13) shows that the Hypoellipse estimates from each sub-array (please note that for practical graphical reason, together with the error ellipse, a line connecting these location estimates with the sub-arrays barycentre is also shown in Figure 13) are characterized by a very large error, being several tens of kilometres from the optimal location provided by Atakan and Sorensen (2006). Note that, as we are still aiming at mimicking REL, when the intersection of the error ellipses is considered (Figure 12), the underlying area is also very large and does not include the Atakan and Sorensen (2006) epicentre estimation.

Finally, we point out that the importance of the REL localization for the two events analysed must be evaluated while taking into consideration that, although these events were relatively small in size (Atakan and Sorensen, 2006), they probably occurred along the SE-part of the North Boundary fault which, based on macroseismic observations and available instrumental records, was where there was a previous major earthquake with a surface magnitude of 6.4 that occurred on September 18, 1963 (e.g., Taymaz *et al.*, 1991).

5. Discussion and conclusion

We have proposed a seismic antenna procedure for rapid earthquake localization based on the cross-correlation of the first P-wave arrivals in the time domain. The REL method aims to be useful in those circumstances where the seismogenic area is outside of a network of seismic stations, a situation for which other localization procedures might be less effective.

The procedure has been generalized in order to be effective for cases of nearby sources which introduce circular wave-fronts incoming to the arrays and for incoherent or partially coherent arrays. This is done by the use of normalized analytical Gaussian functions centred on the first P-wave arrival time. In the application of REL to the large and dense IERRS network, it has been possible to optimize the algorithm to follow a more general framework where different sub-arrays of stations provide their own localization estimates and the epicentral area is found by a triangulation-like principle in the final stacked coherency map.

Using synthetic data with the IERRS network geometry as the reference, the REL's performance has been tested for different scenarios. Moreover, tests have also been performed to evaluate the reliability of the procedure while considering the failure of certain numbers of the IERRS's stations. We have verified that the REL provides very good reliability for the rather extreme case of 25% of stations failing in each sub-array. It is worth noting that for rapid response purposes, the robustness of the procedure is a very important property. Further tests with synthetic data showed that using REL allows high-quality epicentral localization to be obtained in the Marmara Sea region for a wide range of azimuths and distances, while, due to the IERRS's geometry, only particular azimuths lead to significant errors in the distance estimates.

The analysis of real data from IERRS for two events that occurred in the Marmara Sea area highlights how REL is able to obtain area estimates of the location of an earthquake's epicentre that are useful for RR systems. Such results confirm that in the presence of a dense array of sensors and the knowledge of the likeliest occurrence of earthquakes outside of the network, seismic antenna methods can be useful for obtaining rapid, almost real time, epicentre location estimates.

Regarding the outcomes obtained, we believe that the REL approach could feasibly be applied for EW and RR activities (e.g., shake map computation). However, we admit that the REL application and suitability for EW purposes in Istanbul would only be possible under the condition that the events occur at least some tens of kilometres from the city. In fact, the applicability of any method for EW purposes requires that certain scientific and technical conditions are fulfilled. Concerning the most important technical constraint, that is the computation time required by REL, at the moment we can provide only a partial assessment. As we have verified by tests with synthetic data, the method is already effective and the analysis can start at each sub-array when at least 75% of the stations of the sub-array have triggered on the P-waves. However, a drawback is that, being a seismic antenna approach, the time necessary for triggering all of the stations in a sub-array leads to a reduction in the lead-time. The value of this wasted time will depend on the efficiency in the telemetry of information. However, considering the ongoing rapid improvements in telemetry technology and the general decrease in communication costs, as demonstrated by the SOSEWIN system installed in Istanbul (Fleming *et al.,* 2009), we believe that in the near future all the networks could be operated in real time, making the performance of real-time seismic analyses methods such as REL a possibility.

In the near future, it is planned to review the design of the algorithm in order to make it faster and more suitable for real-time operations. Therefore, only after the improvements in the code's efficiency are implemented and a period of tests with both real and synthetic data will it be possible to better design the REL for its application to the Istanbul situation, which is a case where the distance between the likely occurrence of earthquakes and areas requiring warning are at the threshold of allowing a long enough lead time for early warning.

In future applications of this method to additional datasets, the use of three components ground motion data and assessing the influence of source depths will be assessed. Moreover, the importance of the presence of additional arrays in the Marmara Sea area, for example in the Yalova peninsula, for improving the REL performance will be tested, and in doing so, hopefully improve seismic hazard mitigation for the megacity of Istanbul.

REFERENCES

Allen, R., & Kanamori, H, 2003. The potential for Earthquake Early Warning in Southern California, *Science*, 300, 786-789. doi: 10.1126/science.1080912.

Allen, R.M., 2007. The ElarmS earthquake early warning methodology and its application across California. In "Earthquake Early Warning Systems", P. Gasparini, G. Manfredi, J. Zschau (Eds), p. 21-44, Springer, ISBN-13 978-3-540-72240-3.

Almendros, J., Ibanez, J.M., Alguacil, G., & Del Pezzo, E., 1999. Array analysis using circular-wave-front geometry: an application to locate the nearby seismo-volcanic source, *Geophys. J. Int.*, 136, 159-170.

Almendros, J., Chouet, B., & Dawson P., 2001a. Spatial extent of a hydrothermal system at Kilauea Volcano, Hawaii, determined from array analyses of shallow long-period seismicity. 1. Method, *Journal of Geophysical Research*, 106, 13565-13580.

Almendros, J., Chouet, B., & Dawson P., 2001b. Spatial extent of a hydrothermal system at Kilauea Volcano, Hawaii, determined from array analyses of shallow long-period seismicity. 2. Results, *Journal of Geophysical Research*, 106, 13581-13597.

Ansal, A., Laue, J., Buchheister, J., Erdik, M., Springman, S.M., Studer, J., & Koksal, D., 2004. Site characterization and site amplification for a seismic microzonation study in Turkey, *Proceedings of the 11th Intl. Conf. On Soil Dyn. & Earthquake Engng. (11th ICSDEE) & the 3rd Intl. Conf. On Earthquake Geotech. Engng. (3rd ICEGE)*, January 7-9, Berkeley, CA, 2004: 53-60.

Armijo, R., Pondard, N., Meyer, B., Uçarkus, G., Mercier de Lépinay, B., Malavieille, J., Dominguez, S., Gustcher, M.A., Schmidt, S., Beck, C., Çagatay, N., Çakir, Z., Imren, C., Eris, K., Natalin, B., Özalaybey, S., Tolun, L., Lefèvre, I., Seeber, L., Gasperini, L., Rangin, C., Emre, O., and Sarikavak, K. , 2005. Submarine fault scarps in the Sea of Marmara pull-apart (North Anatolian Fault): Implications for seismic hazard in Istanbul, *Geochem. Geophys. Geosyst.*, *6*, Q06009, doi:10.1029/2004GC000896.

Atakan, K., & Sorensen, M.B., 2006. Potential of vulnerability and seismic risk, *Deliverable no.27. Large Earthquake Faulting and Implications for the Seismic Hazard Assessment in Europe: The Izmit-Düzce earthquake sequence of August-November 1999 (Turkey, Mw 7.4, 7.1)*. EC Project EVG1-CT-2002-00069.

Birgören, G., Özel, O., Fahjan, Y., & Erdik, M., 2004. Determination of site effects in Istanbul area using a small earthquake record of dense strong motion network, *XXIX General Assembly of the European Seismological Commission, Potsdam, Germany, poster no. 249*.

Birgören, G., & Özel, O., 2006. Determination of site effects and ground motion lengthening in Istanbul area derived from small earthquake recordings. *Proceedings of the 8th U.S. National Conference on Earthquake Engineering 2006; April 18-22, San Francisco, California, USA, Paper No. 1908*.
Crotwell, H. P., T. J. Owens, and J. Ritsema (1999). The TauP Toolkit: Flexible seismic travel-time and ray-path utilities, Seismological Research Letters 70, 154–160.

Del Pezzo, E., La Rocca, M., & Ibanez, J., 1997. Observation of high frequency scattered waves using dense arrays at Teide volcano, *Bull. Seism. Soc. Am.*, **87**, 1637-1647.

Efron, B., & Gong, G., 1983. A Leisurely Look at the Bootstrap, the Jackknife, and Cross Validation, *The American Statistician*, 37, 1, 36-48.

Erdik, M., Aydinoglu, N., Fahjan, Y., Sesetyan, K., Demircioglu, M., Siyahi, B., Durukal, E., Ozbey, C., Biro, Y., Akman, H., & Yuzugullu, O., 2003a. Earthquake Risk Assessment for Istanbul Metropolitan Area, *Earthquake Engineering and Engineering Vibration*, vol. 2, No. 1, 1-27.

Erdik, M., Fahjan, Y., Özel, O., Alcik, H., Mert, A., & Gul, M., 2003b. Istanbul Earthquake Rapid Response and the Early Warning System, *Bulletin of Earthquake Engineering*, 1, 157-163.

Fleming, K., Picozzi, M., Milkereit, C., Kuehnlenz, F., Lichtblau, B., Fischer, J., Zulfikar, C., Ozel, O., and the SAFER and EDIM working groups (2009). The Self-Organising Seismic Early Warning Information System (SOSEWIN). *Seismological Research Letters.* **80**, 5, **755-771**.

Fletcher, J.B., Spudich, P., & Baker, L.M., 2006. Rupture Propagation of the 2004 Parkfield, California, Earthquake from Observation at the UPSAR, *Bull. Seism. Soc. Am.*, **96**, n. 4B, 2006, S129-S142.

Frankel, A., Hough, S., Friberg, P., & Busby, R., 1991. Observation of Loma Prieta aftershocks from a dense array in Sunnyvale, California. *Bull. Seism. Soc. Am.*, **81**, 1900-1922.

Gibbons, S.J., & Ringdal, F., 2006. The detection of low magnitude seismic events using array-based waveform correlation, *Geophys. J. Int.*, 165, 149-166.

Gibbons, S.J., Ringdal, F., & Kvaerna, T., 2008. Detection and characterization of seismic phases using continuous spectral estimation on incoherent and partially coherent arrays, *Geophys. J. Int.*, 172, 405-421.

Goldstein, P., & Archuleta, R., 1991. Deterministic Frequency-Wavenumber Methods and Direct Measurements of Rupture Propagation During Earthquakes Using a Dense Array, *Journal of Geophysical Research*, **96**, N.B4, 1991, 6187-6198.

Kanamori, H., 2005. Real-Time Seismology and Earthquake Damage Mitigation, *Annu. Rev. Earth Planet.*, 33: 195-214, doi: 10.1146/annurev.earth.33.092203.122626.

Karabulut, H., Bouin, M-P., Bouchon, M., Dietrich, M., Cornou, C., & Aktar, M., 2002. The seismicity in the eastern Marmara Sea after 17 August 1999 Izmit Earthquake *Bull. Seism. Soc. Am.*, 92, 387-393.

Klein, F.W., 2002. User's guide to HYPOINVERSE-2000, a FORTRAN program to solve 605 earthquake locations and magnitudes. U. S. Geological Survey Open File Report 02-606 171 Version 1.0.

Krüger, F., & Ohrnberger, M., 2005. Tracking the rupture of the Mw=9.3 Sumatra earthquake over 1,150 km at teleseismic distance, *Nature*, 435, 16, 937-939, Doi:10.1038/nature03696.

Lahr, J.C., 1999. Quick-start manual for Hypoellipse, a computer program for determining local earthquake hypocentral parameters, magnitude, and first-motion pattern (Y2K compliant version), Version 1.0, U.S. Department of the Interior U.S. Geological Survey.

Mori, J., Filson, J., Cradwick, E., Borcherdt, R., Amirbekian, R., Aharonian, V., & Hachverdian, L., 1994. Measurements of P and S wave-front from the dense three-dimensional array at Garni, Armenia, *Bull. Seism. Soc. Am.*, **84**, 1089-1096.

Özel, O., Sasatani, S., Kudo, K., Okada, H., Kanno, T., Tsuno, S., Yoshikawa, M., Noguchi, S., Miyahara, M., Goto, H., (2004). Estimation of S-wave velocity structure in Avcilar-Istanbul from array microtremor measurements. *Journal of the Faculty of Science, Hokkaido University 7, Geophysics* 12, 115–129.

Picozzi, M., Strollo, A., Parolai, S., Durukal, E., Özel, O., Karabulut, S., Zschau, J., and M. Erdik, M. (2009). Site characterization by seismic noise in Istanbul, Turkey. *Soil Dynamic and Earthquake Engineering*, 29, 469– 482, doi:10.1016/j.soildyn.2008.05.007

Ringdal, F., & Kvaerna, T., 1989. A Multi-Channel processing approach to real time network detection, phase association, and threshold monitoring, *Bull. Seism. Soc. Am.*, **79,** 1927-1940.

Satriano, C., Lomax, A., & Zollo, A., 2008. Real-Time Evolutionary Earthquake Location for Seismic Early Warning, *Bull. Seism. Soc. Am.*, 98, 1482-1494

Schweitzer, J., Mykkeltveit, S., & Kvaerna, T., 2002. Seismic Arrays, in *IASPEI New Manual of Seismological Observatory Practice*, P. Bormann (Editor), Vol.1, GeoForschungsZentrum Potsdam, Germany, Chapter 9, 51 pp.

Sesetyan, K., Zulfikar, C., Demircioglu, M., Hancilar, U., Kamer, Y., and Erdik, M. (2010). Istanbul Earthquake Rapid Response System: Methods and practices. Soil Dyn. Eartquake Eng., doi:10.1016/j.soildyn.2010.02.012.

Taymaz, T., Jackson, J., &, McKenzie, D., 1991. Active tectonics on the north and central Aegean Sea, *Geophys. J. Int.*, **106**, 433-490.

Tezcan, S.S., Kaya, E., Bal, L.E., &, Özdemir, Z., 2002. Seismic amplification at Avcilar, Istanbul, *Engineering Structures*, **24**, 661-667.

Wessel, P., & Smith, W.H.F., 1991. Free software helps map and display data, *EOS Trans. AGU*, 72, 445-446.

Figure Captions

Figure 1: Performance of the epicentre location algorithm Hypoellipse (Lahr, 1999) when applied to an event that occurred in the Marmara Sea on September 29, 2004, and considering arrival times recorded by the IERRS network. IERRS stations (*gray dots*), coastline (*black line*), schematic representation of faults (*gray lines*), 7 stations from the International Seismological Centre database (*gray squares*), reference epicentre location (*black diamond*), Hypoellipse localizations using P-wave trigger times plus 95% confidence error ellipses (*light grey diamond and dotted line*), Hypoellipse localizations using P and S-wave trigger times plus error ellipse (*dark grey diamond*), Hypoellipse localizations considering the IERRS network plus the 7 extra seismological stations and using both P and S-wave trigger times plus error ellipse (*dark grey diamond and dotted line*).

Figure 2: Flowchart describing the REL procedure. *Top panel*) Sub-arrays of IERRS stations (*grey, white and black dots*), coastline (*black line*), and schematic representation of faults (*gray lines*). *Middle panels*) Coherency maps for the three IERRS sub-arrays, Sub-array stations (*red dots*), REL's epicentre (*green dot*), simulated epicentre (*grey dot*), and schematic representation of faults (*yellow lines*). *Lower panel*) Stacked coherency map, IERRS stations (*red points*), coastline (*black line*), simulated epicentre (*grey point*), and REL estimate (*green point*). Coherency values are indicated by colour of the dots.

Figure 3: *Top panel*) Example of 3D accelerograms for an IERRS station. The portion of the data where the picking on the vertical component of the first P-wave is performed is indicated (*black line*). *Lower panel*) Example of vertical component accelerogram (black line) with the STA/LTA trigger of the first P-wave (red line), and the normalized analytical Gaussian function centred on the first P-wave arrival time (blue line).

Figure 4: Results of the application of REL to synthetic data. *Top-left panel*) Sub-arrays of IERRS stations (*grey, white and black dots*), coastline (*black line*), schematic representation of faults (*gray lines*), and location of epicentres selected for the tests. *Other panels*) Stacked coherency map as in Figure 2 for the different scenarios.

Figure 5: Results of synthetic tests made to evaluate the influence of the IERRS geometry on the epicentre localization. IERRS stations (*red points*). *a)* Percentage error in azimuth. *b)* Percentage error in distance. Errors are indicated by both the colour and size of the dots.

Figure 6: Same as Figure 3, but with for a grid search performed for points located along the faults in the Marmara Sea region and for different scenarios (note these scenarios are different from those assessed in Figure 3).

Figure 7: Results of the Jacknife analysis used to verify the effect of the failure of some stations on the REL reliability. *Left panel* − error rate for azimuth (*light grey squares*), distance (*dark grey diamonds*), and their sum (*black dots*) plus the relative 95% confidence interval as a function of the simulated station failure rate.

Figure 8: *a)* Locations and focal mechanisms of the two earthquakes recorded by the IERRS (*beach ball*) and examined in this work. IERRS stations (*green triangles*) (redrawn from Birgören *et al.,* 2004). *b)* Accelerograms as recorded by the IERRS for the earthquake of May 16, 2004 (Mw = 4.2). The hypocenter of the event is also shown (*beach ball*).

Figure 9: Example of accelerograms (vertical component of ground motion) recorded at a IERRS station (*black line*). STA/LTA trigger time (*red line*).

Figure 10: REL results for the September 29, 2004 event. Standard seismological localization estimate (*grey point*), REL maximum coherency estimate (*green point*), and IERRS stations (*red points*). *a)* Results for the different sub-arrays and exploring the whole area southern of Istanbul. *b)* Stacked coherency map. *c)* Same as *a)* but exploring only points located along the faults in the Marmara Sea region. *d)* Stacked coherency map from maps showed in *c)*. Coherency values are indicated by the colour of the dots.

Figure 11: Same as Figure (10) but from the LUT analysis. The RMS^{-1} is represented by the colour of the dots.

Figure 12: Same as Figure (10) but from the analysis of the May 16, 2004 event.

Figure 13: Hypoellipse (Lahr, 1999) performances for the September 29, 2004 event when applied mimicking the REL approach. IERRS stations subdivided in sub-arrays (*red, blue, green dots*), coastline (*black line*), schematic representation of faults (*gray lines*), reference epicentre location (*black diamond*), location estimates from the different sub-arrays (*light, medium, and dark gray diamonds*), 95% confidence error ellipses (*dotted lines*), area corresponding to the intersection of the error ellipses (*light gray shaded area*), and lines connecting the epicentre location estimates with their sub-arrays barycentre (*black lines*).
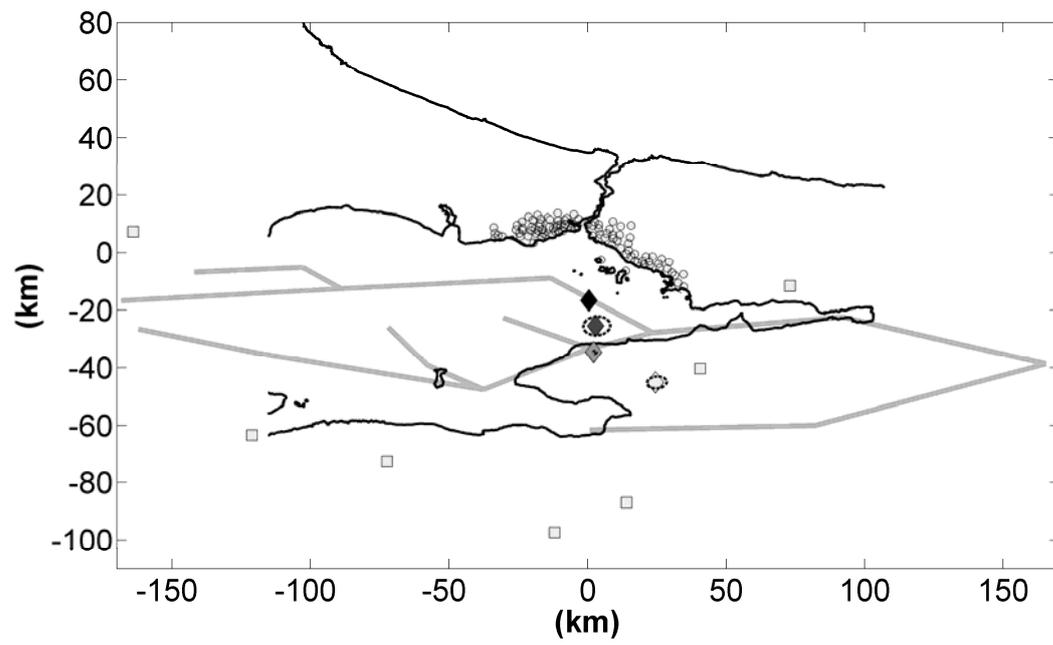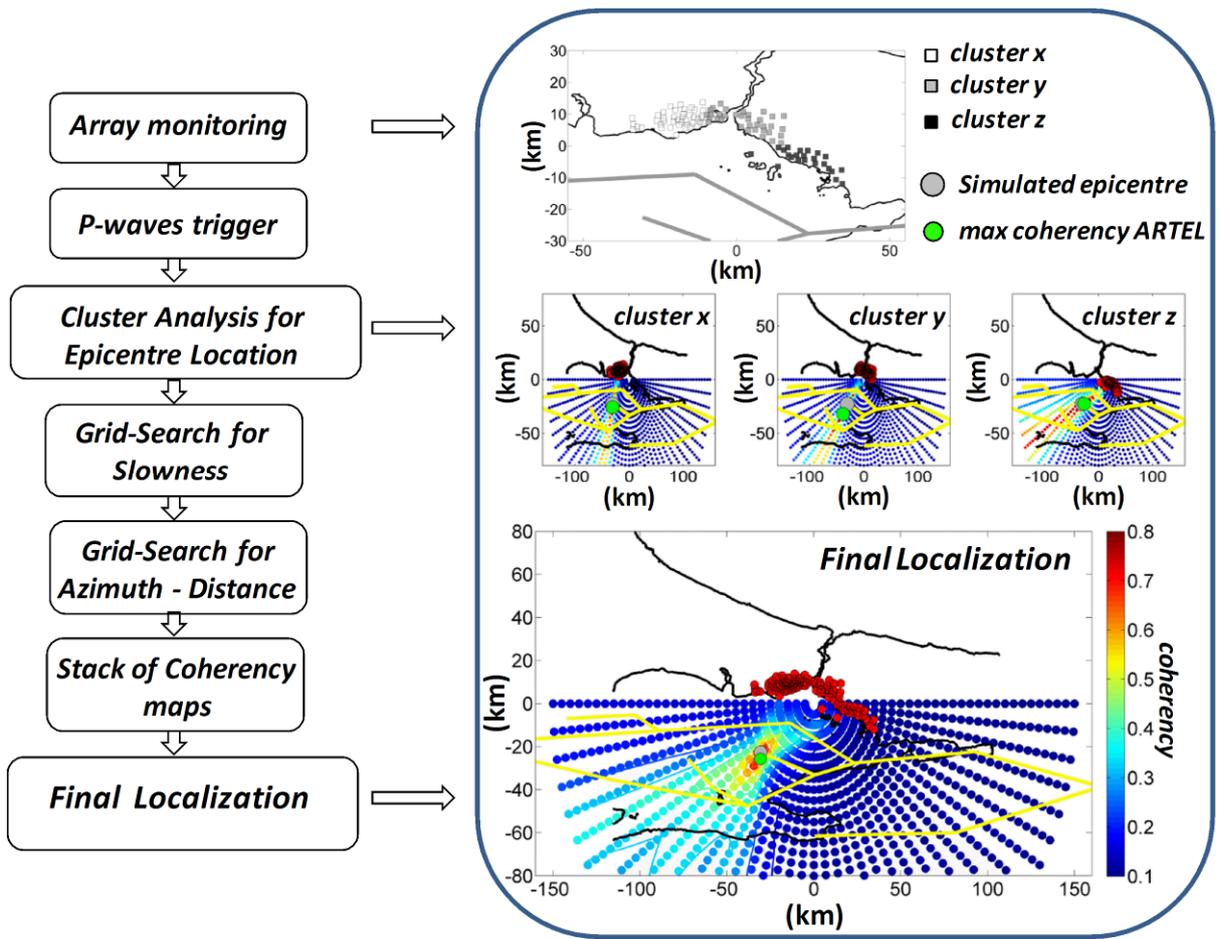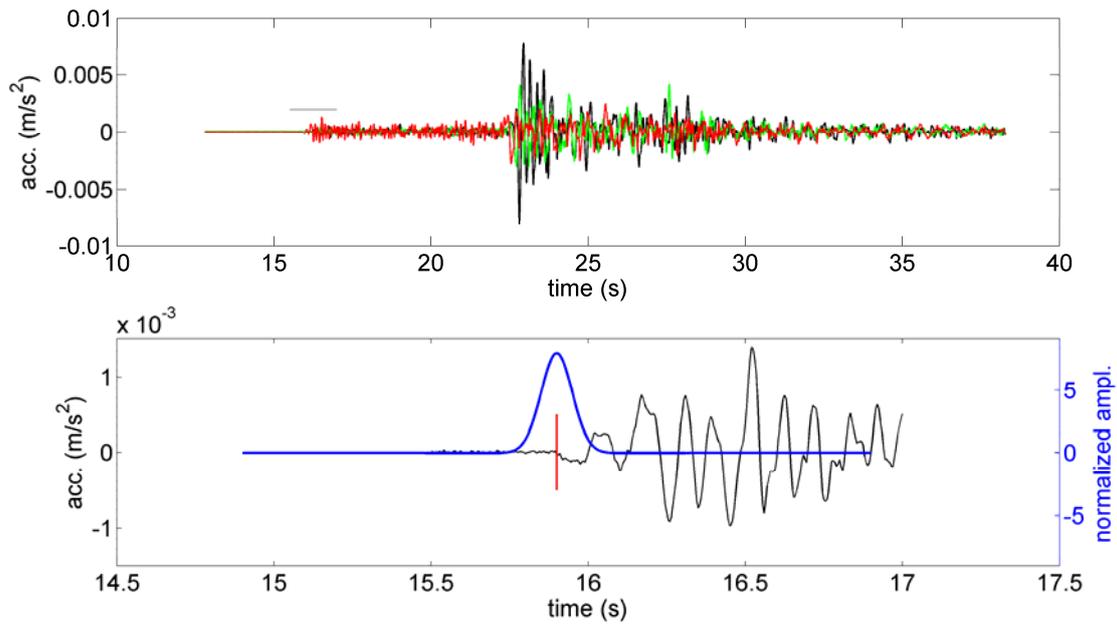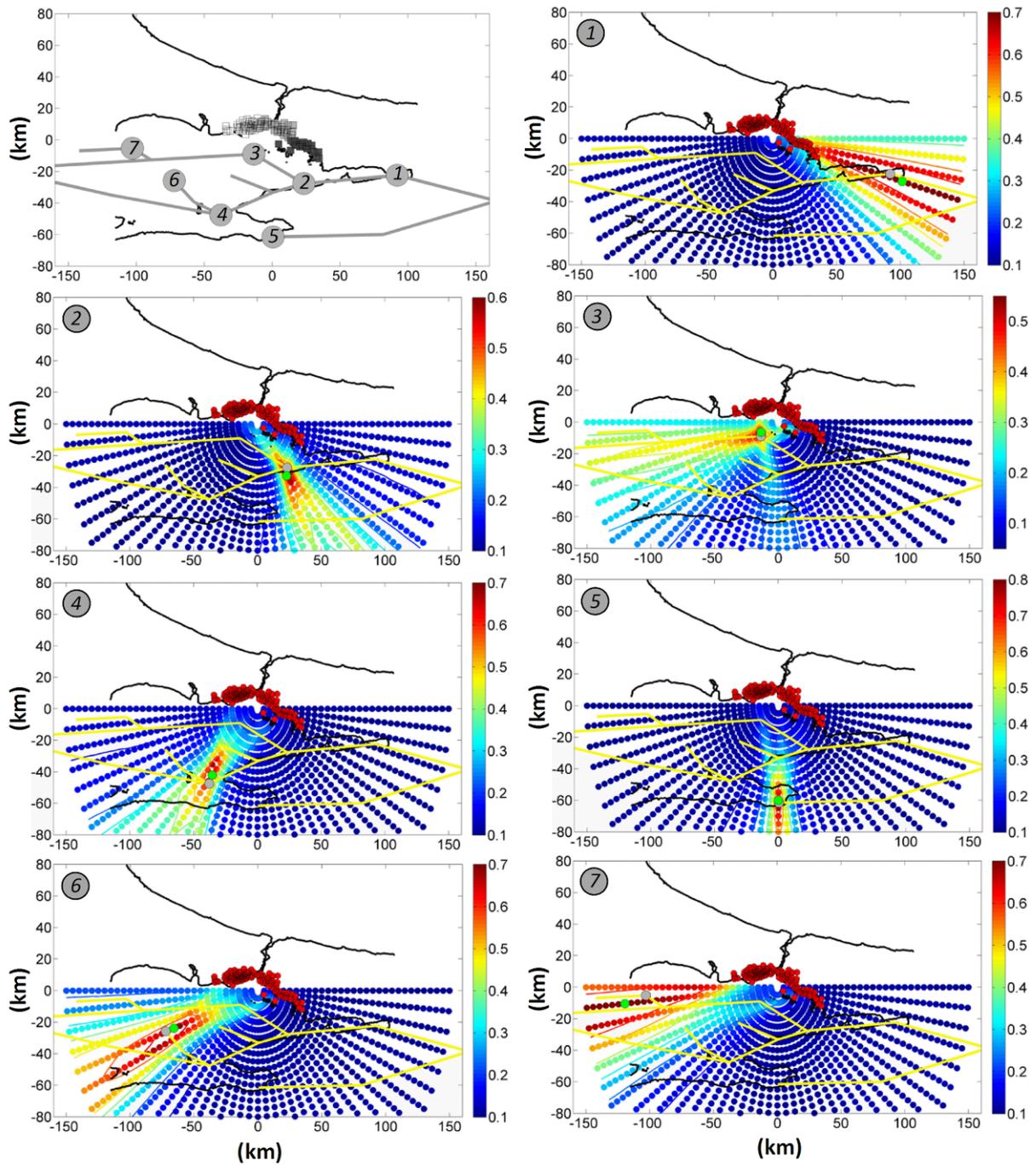
Figure 1

Figure 2

Figure 3

Figure 4
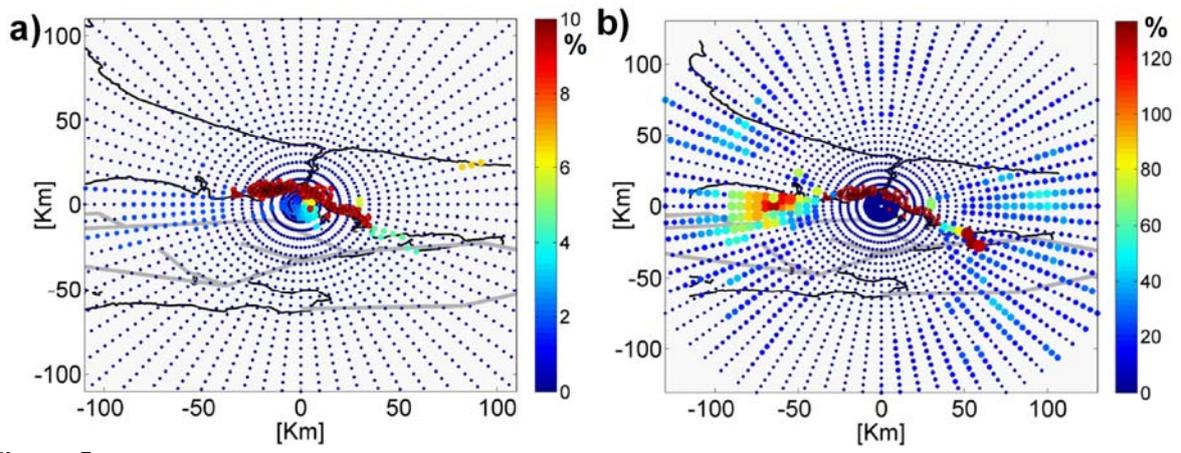
Figure 5
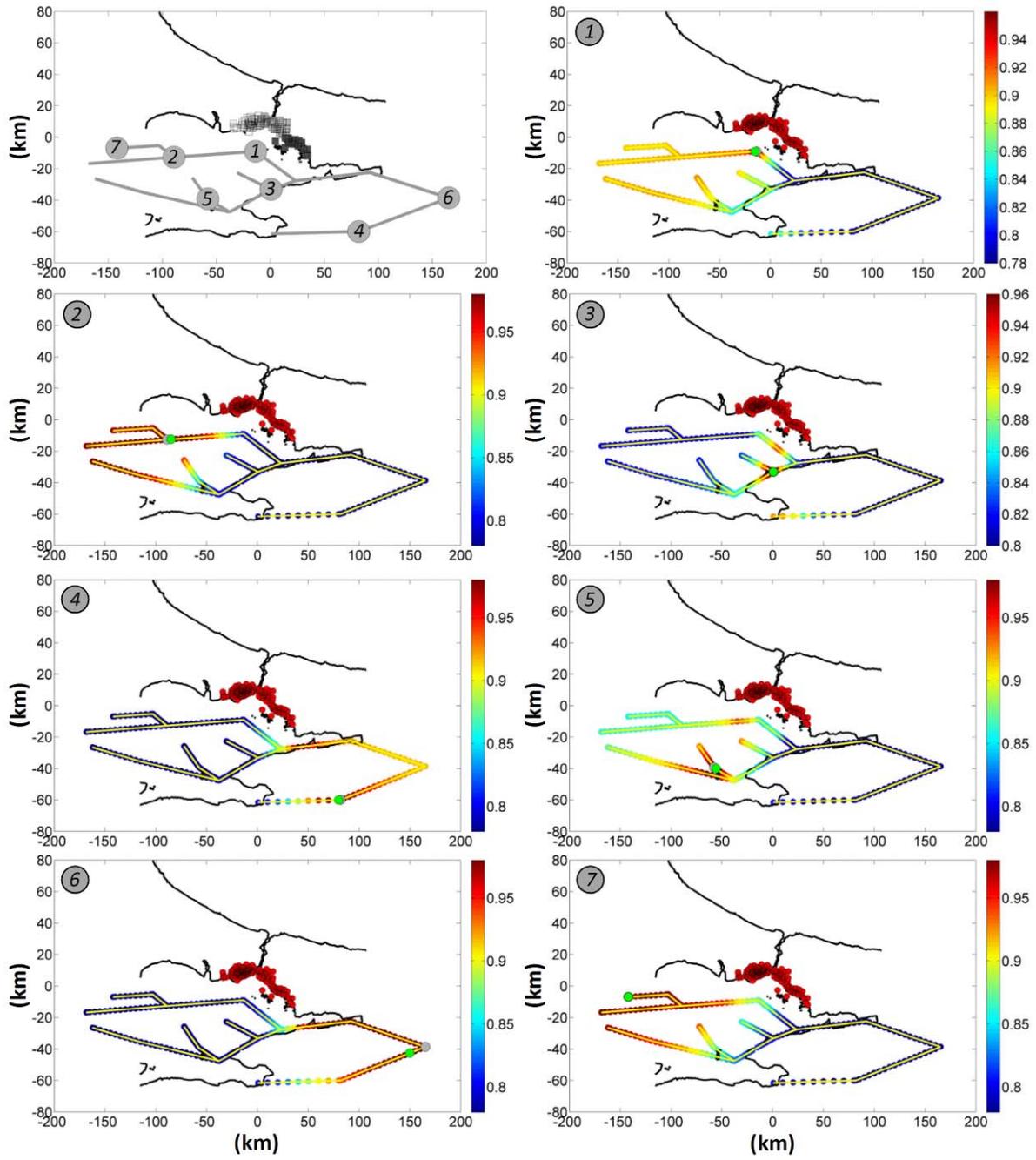
Figure 6
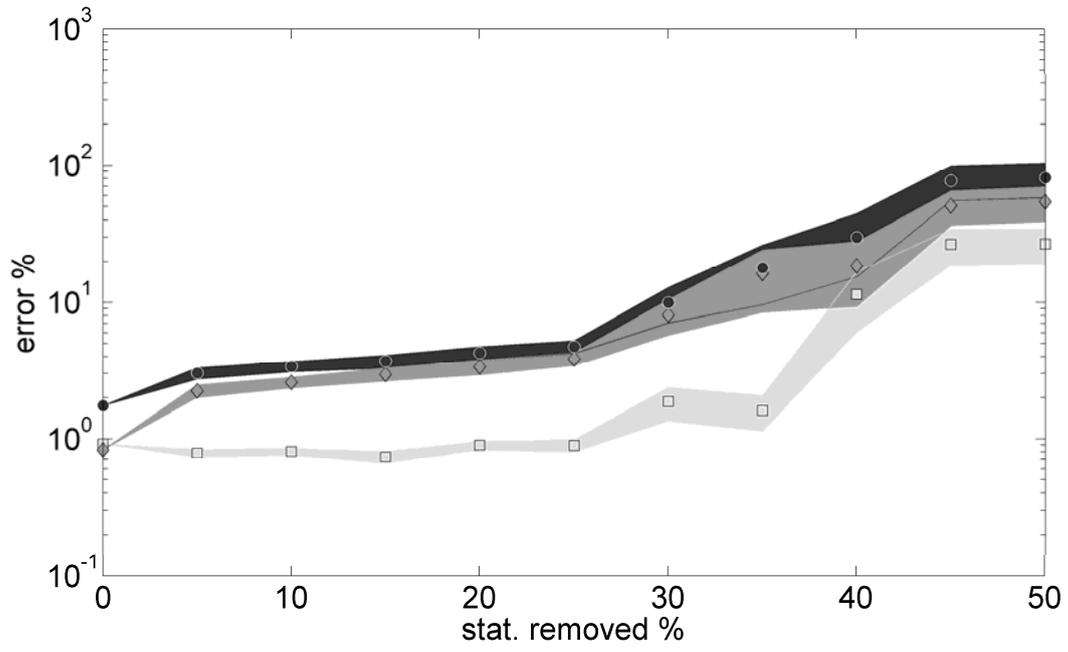
Figure 7
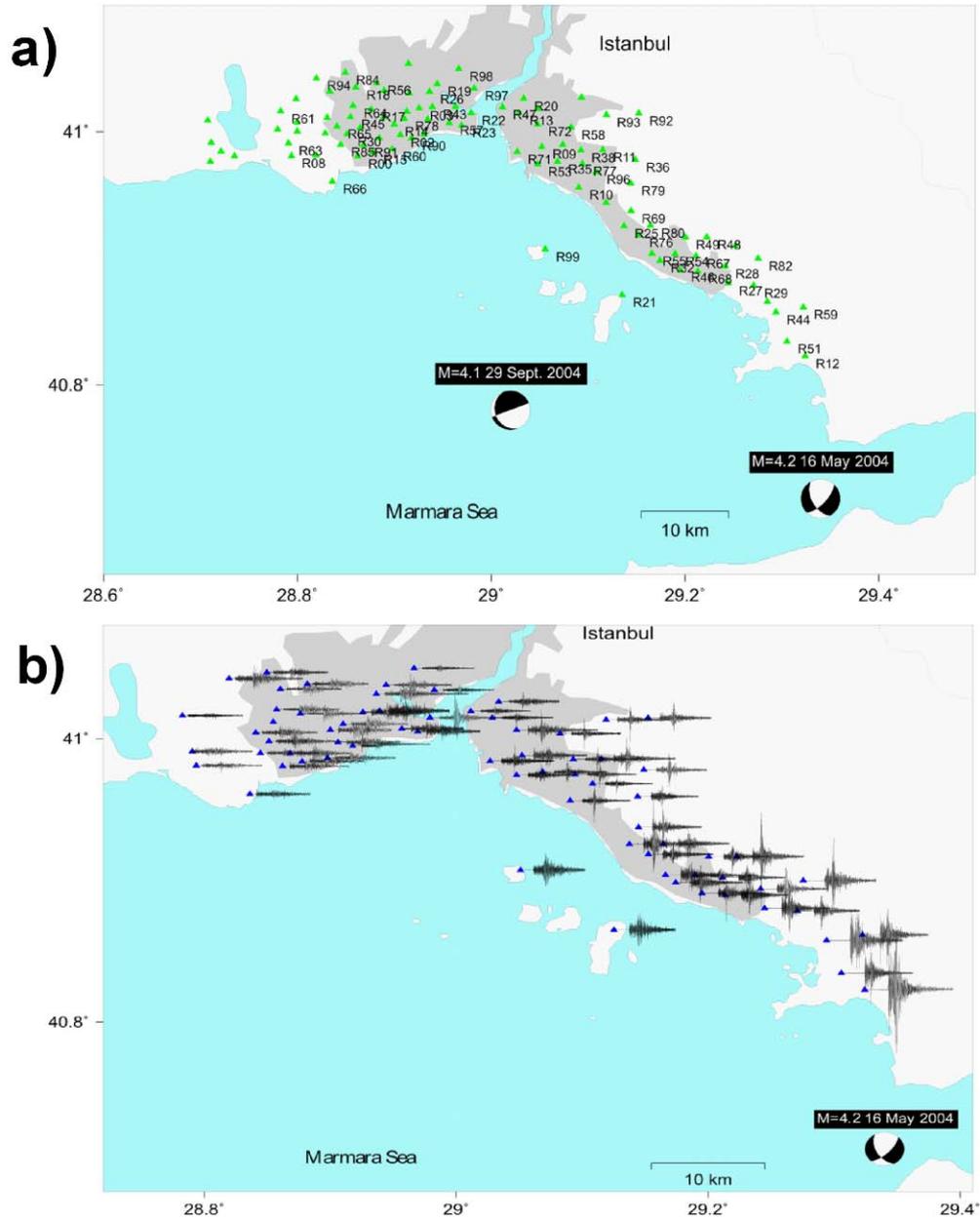
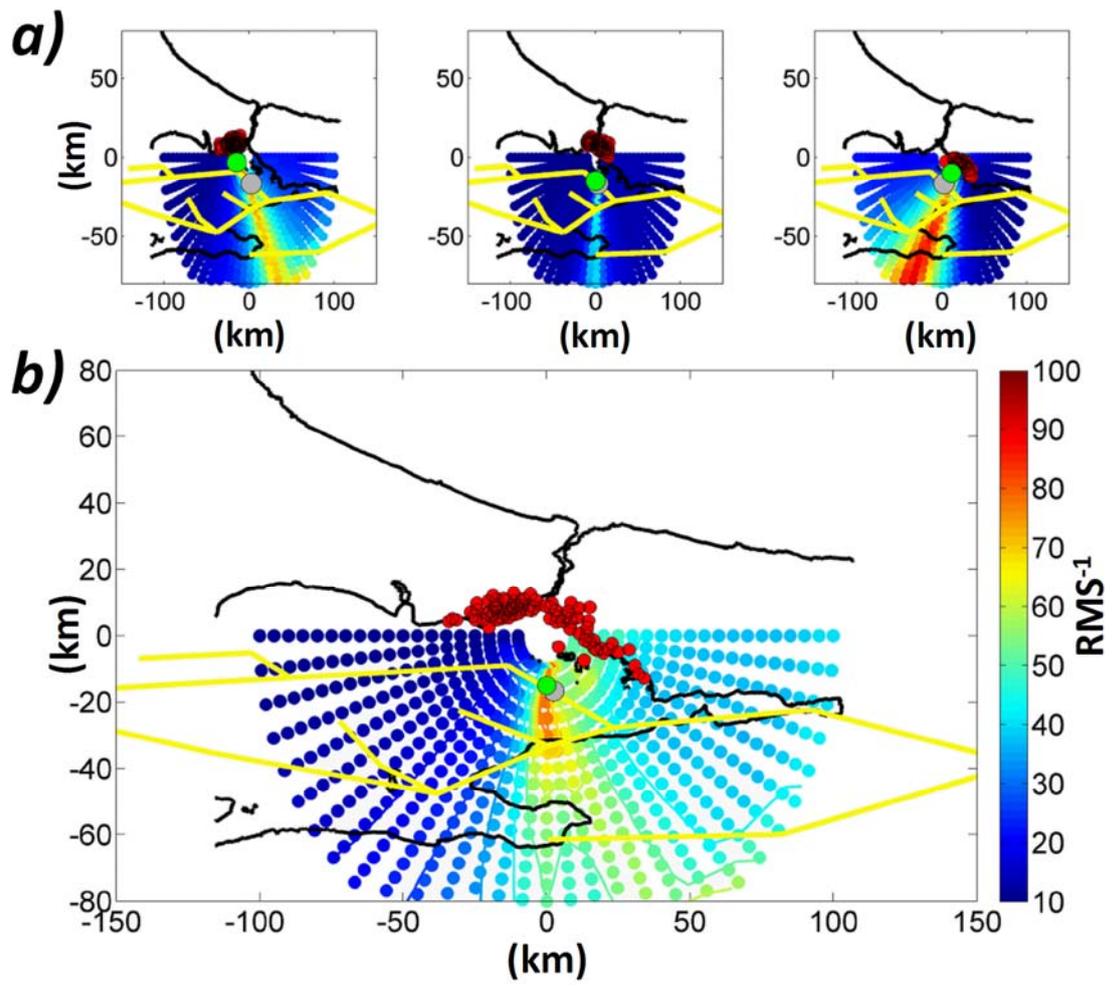**Figure 8**
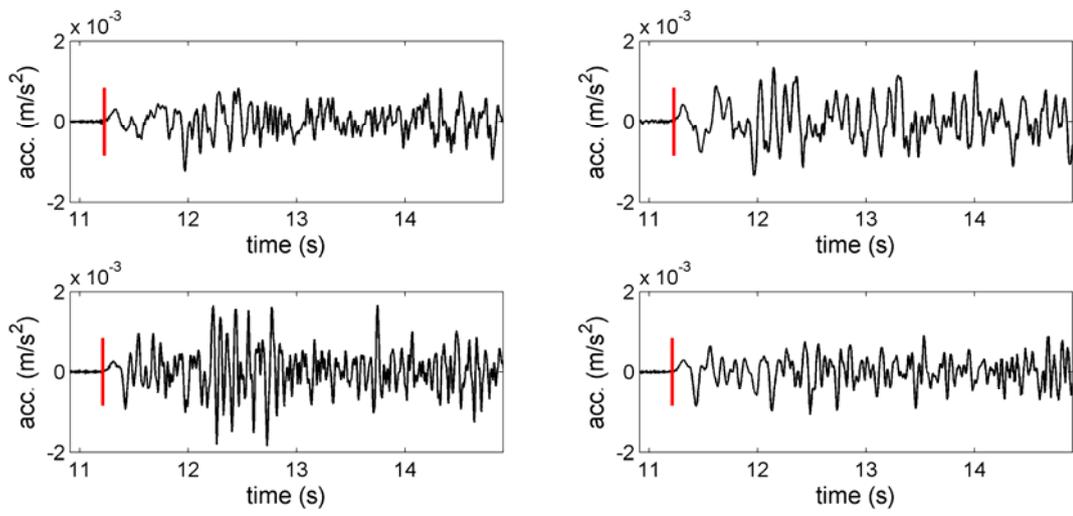
Figure 9
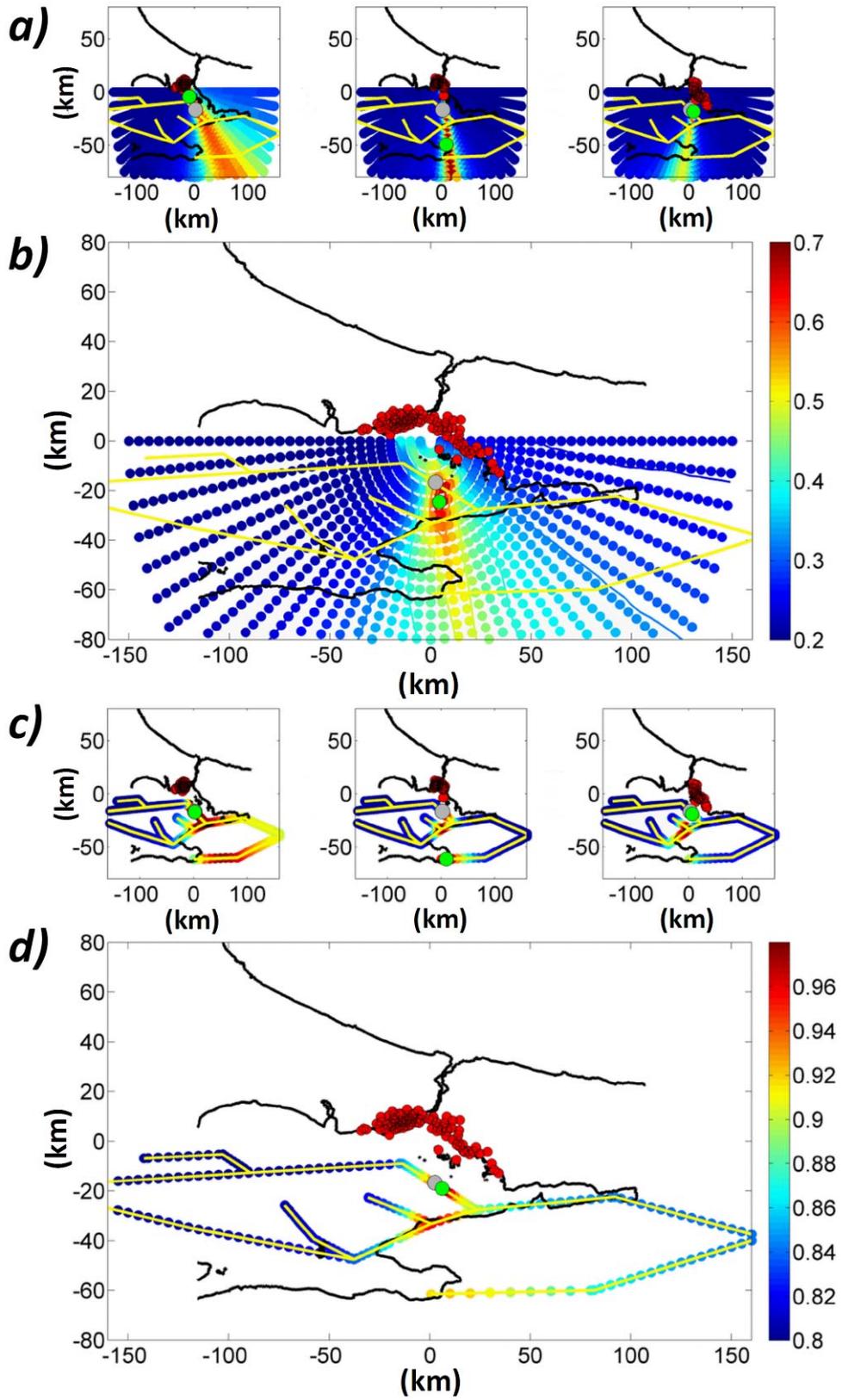
Figure 10

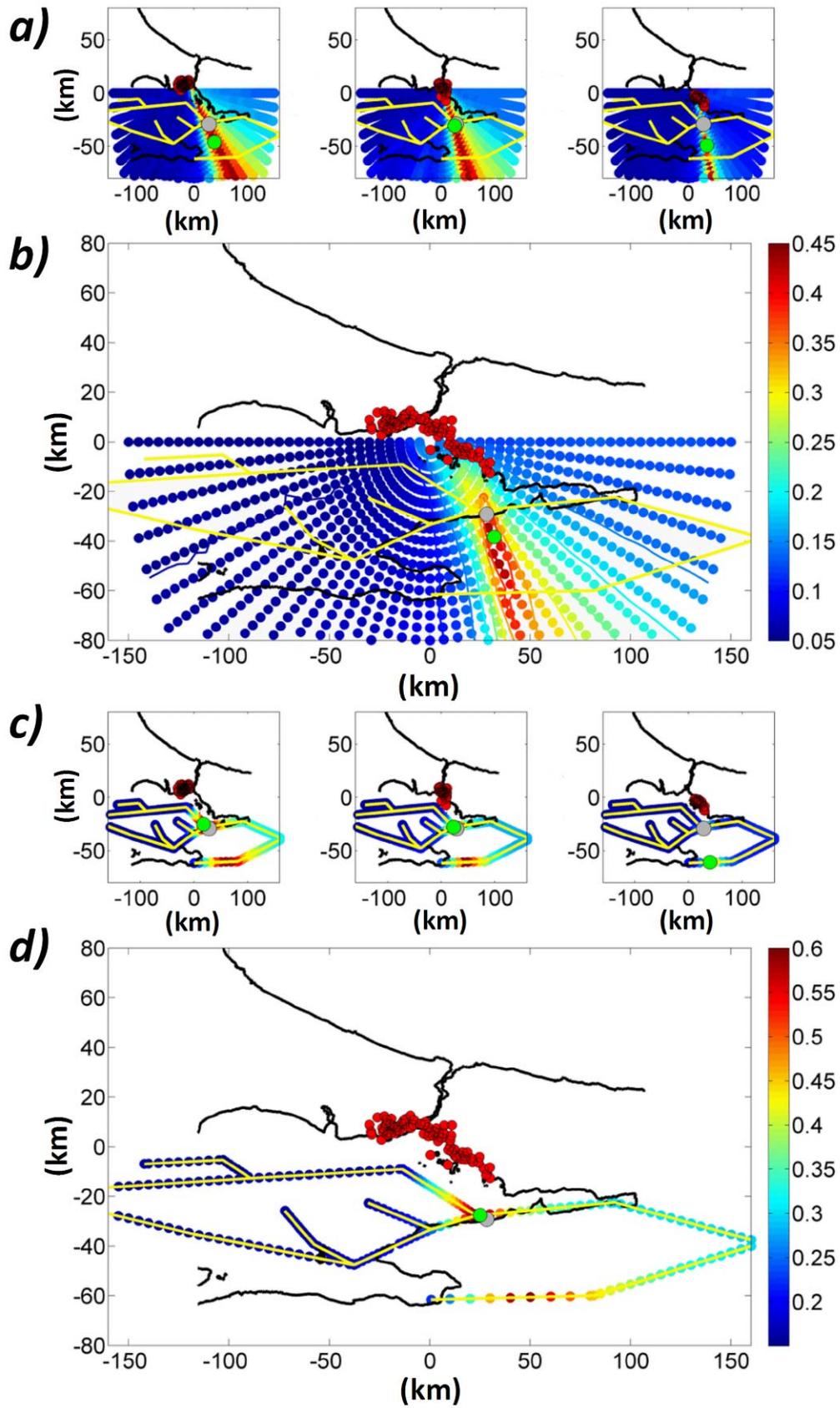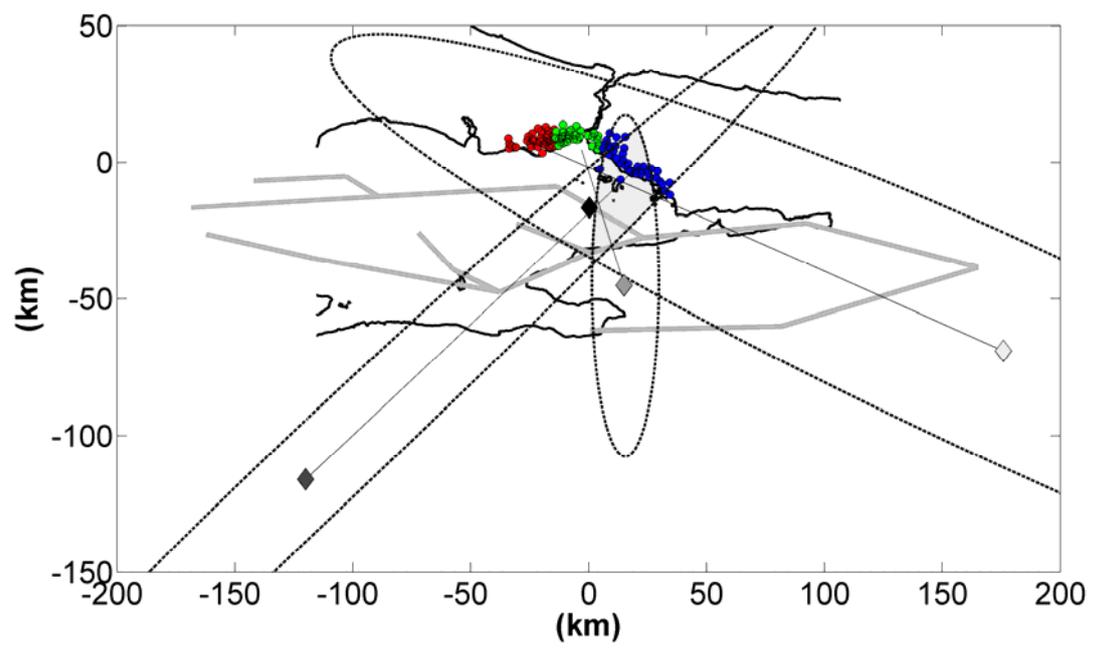**Figure 11**

Figure 12

Figure 13

Table

Table 1: P-wave and S-wave velocity model (Karabulut *et al.,* 2002) used in the simulations

P-waves (km/s)	S-waves (km/s)	Depth (km)
2.25	1.1	0
5.7	3.2	1.1
6.1	3.6	6
6.8	3.8	20
8	4.5	33